Consciousness-related interactions in a double-slit optical interferometer

Gabriel Guerrer*
Instituto de Psicologia, Universidade de São Paulo, São Paulo, Brasil

August 24, 2017

Abstract

Motivated by a series of reported experiments and their controversial results, the present work investigated if volunteers could causally affect an optical double-slit system through mental efforts alone. The participants task alternated between intending the increase of the (real-time feedback informed) amount of light diffracted through a specific single slit and relaxing any intention effort. The 160 data sessions contributed by 127 volunteers revealed a statistically significant 6.37 sigma difference between the measurements performed in the intention versus the relax conditions ($p = 1.89 \times 10^{-10}$, $es = 0.50 \pm 0.08$), while the 160 control sessions conducted without any present observer resulted in statistically equivalent samples ($z = -0.04$, $p = 0.97$, $es = 0.00 \pm 0.08$). The results couldn't be simply explained by environmental factors, hence supporting the previously claimed existence of a not yet mapped form of interaction between a conscious agent and a physical system.

1 Introduction

One of the hardest problems still unsolved by humanity concerns the nature of consciousness and its relationship to matter [1]. The millennial old debate, currently addressed by the philosophy of mind, proceeds asking if there's a more fundamental aspect to reality, what are their properties and how do they interact.

The first time physicists seriously considered the possibility of consciousness being a subject of their responsibility, coincided with the developments of quantum mechanics in the 20$^{\text{th}}$ century. In particular, the question on how the superposition state is reduced to a definite observed state, known as the quantum measurement problem, led some scientists [2–4] to associate such abrupt transitions with a subjective knowledge increase. According to that interpretation, the conscious agent played an essential role in promoting the state reduction when experimenting on the acquired information.

The question evolved into a controversial philosophical and theoretical debate [5–11] to the present-day, where the majority stands for the opposite view, denying the necessity of the "extra-physical" consciousness ingredient in quantum physics [12]. Data in support of the leading view is found in "which-path" experiments, reported and discussed by [13]. Those experiments reveal that a sufficient condition for a superposition state collapse is a "which-path" information availability, even when theoretically obtainable but not effectively measured. The provided counter-examples may lead to the conclusion that information reaching human consciousness is not a mandatory step for state reduction.

Although a strong role for human consciousness in the quantum measurement problem may be ruled out, still, a weaker but not less important role can be investigated: if the right conditions

*guerrer@usp.br

are met, can consciousness collapse the superposition state? Or, more generally, is there any sort of interaction between consciousness-related mental states and quantum systems?

The experimental efforts to address the above questions are dated back to the 70's with the use of random number generators. These devices explore quantum effects as radioactive decay and tunneling to produce truly random binary numbers. In those studies, participants tried to directionally bias the 0 or 1 outcomes through their mental intention, while (usually) being real-time informed about the measured values. Two major meta-analyses have been reported [14, 15], where both resulted in statistical evidence for the investigated goal-oriented interaction. Although significant, the latter concluded that the effect could be more simply explained by an artifact caused by non-significant unpublished studies, what was contested by the authors of the first meta-analysis [16].

The first use of a double-slit interferometer as a target in a similar experimental protocol is attributed to [17]. In the standard double-slit system if a partial which-path information is obtained through extra measurements, one expects as a consequence a reduction in the interference component [18]. The mentioned study investigated the fringe visibility (a measure of the interference component) variation according to the participant's intention. Two experiments were presented, one supporting the interaction hypothesis and the other conforming to chance expectations.

Of particular interest to the present work are the double-slit experiment series [19–22] presented by Dean Radin and his collaborators. Those results are remarkable in the sense that most of the pre-planned experiments resulted in statistically significant evidence supporting the investigated interaction. Their findings, across the work series, claim that the observed effects: a) globally support the *psychophysical* interaction hypothesis, i.e. the causal effect of participant's intention in the optical system (the mind-matter interaction nomenclature is also used); b) cannot be explained as procedural or analytical artifacts, as the control sessions (without participants present) resulted in no significant differences between the intention active and intention absent epochs; c) are stronger for participants with contemplative practices training, e.g. meditation; d) show a positive correlation to the participant's score obtained in the absorption questionnaire [23] measuring the degree of immersion that one can reach when performing a task; e) show a positive correlation to α desynchronization, a marker of increased attention measured by an electroencephalogram device; f) are retro-causal, i.e. obtainable even when the participant acts in previously recorded data that was kept unseen by any participant or the experimenter prior to the session; g) don't depend on distance, occurring even when the participant (not physically present in the experimental room) tries to exert their action on a distant real-time data collection, while receiving the feedback information streamed via the internet. As result, the effect sizes obtained doesn't display a significant correlation to the participant distance to the apparatus.

Inspired by Radin et al. challenging claims in the face of the present scientific world view, the current experiment tried to replicate their first four findings (a discussion concerning c) and d) results is outside the scope of the present work and will be left for a future publication) using a similar protocol and a modified setup/analysis as described below.

2 Results

2.1 Double-slit optical system

The double-slit system geometry is presented in Fig. (1). According to the experimental setup described in Section 4.1, after traveling 38 cm the diverging laser beam reaches the double-slit region (in a good approximation) as a monochromatic plane wave of λ wavelength. The wavefront is then diffracted by the two rectangular apertures with respective widths of s_1 and s_2, which are separated by a d length. The distance from slit j center to a x point in the

camera sensor is given by $r_j = \sqrt{y^2 + x_j^2}$, where: $j = 1, 2$; $x_1 = (x - x_0) + (s_1 + d)/2$; $x_2 = (x - x_0) - (s_2 + d)/2$; and x_0 is the centrally-symmetric position between both slits.

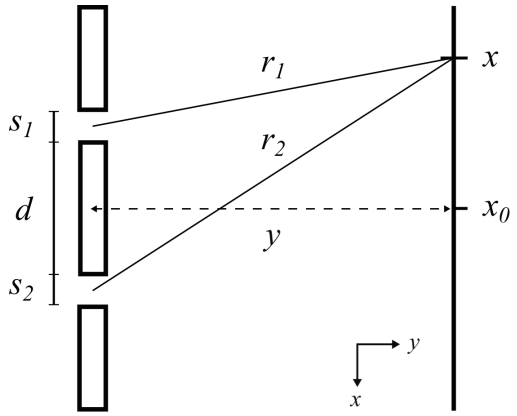

Figure 1: Top view of the double-slit system geometry. The double-slit xz plane is placed at a fixed y distance from the camera sensor xz plane.

According to the scalar diffraction theory [24, p. 75], the wavefield strength U at a point x can be expressed as a superposition of U^0 intensity spherical waves emanating from every point within the diffraction aperture. The Huygens-Fresnel principle (as predicted by the first Rayleigh-Sommerfeld solution) followed by a Fraunhofer approximation, results in the following intensity after a single slit:

$$U_j(x) = -i\,U_j^0\,\frac{h\,s_j}{\lambda\,y}\,\exp\left\{i\,\left[\theta_j + k\,y + \frac{k}{2y}\,x_j^2(x)\right]\right\}\,\frac{\sin\beta_j(x)}{\beta_j(x)}, \qquad (1)$$

$$\beta_j(x) = \frac{k\,s_j}{2y}\,x_j(x),$$

where $k = 2\pi/\lambda$, h is the slit height and a θ_j phase is introduced to represent a possible small rotation of the slit plane over the z axis. The measured light intensity I in the CCD sensor plane is given by the two slit field superposition $\left|1/\sqrt{2}\,U_1 + 1/\sqrt{2}\,U_2\right|^2$, and in more detail to:

$$I(x) = \frac{1}{2}\,I_1(x) + \frac{1}{2}\,I_2(x) + \cos\left\{\frac{k}{2y}\,\left[x_2^2(x) - x_1^2(x)\right] + \theta_r\right\}\,\sqrt{I_1(x)\,I_2(x)} + DC, \qquad (2)$$

$$I_j(x) = U_j(x)\,U_j^*(x),$$

where $\theta_r = \theta_2 - \theta_1$, and DC represent the dark current noise in the camera CCD. The first and the second terms are the *diffraction* components and the third term is the *interference* component. All components together form an *interference pattern*, as exemplified in Fig. (6).

A least square curve fitting procedure using Eq. (2) is applied to extract the physical parameters of the experimental setup. The data sample used consists of 100 CCD frames (equally time spaced) obtained from each of the 130 control sessions formed by experiments 1, 3, 4 and 5 (experiment 2 was left out for providing slightly deviant values; for the experiment definitions see Section 2.3). For practical purposes Eq. (2) is rewritten: $h\,U_1^0$ is factored out from the three first members and $U_r = U_2^0/U_1^0$ is introduced in the next two; the x value is converted to a discrete set using the relationship $x = (i - i_0)\,\Delta p$, where $i = 0, \ldots, 1263$ and Δp is the pixel size. The extracted parameters are shown in Tab. (1).

2.2 Hypothesis

The complementarity principle in quantum mechanics states that one can observe either the wave or the particle properties of light, but not both simultaneously. In the double-slit experi-

par	mean	std	unit
y	30.447	0.022	mm
s_1	12.55	0.13	μm
s_2	12.13	0.17	μm
$h\,U_1^0$	241	3	mm
DC	360	40	–
U_r	0.963	0.017	–
θ_r	-0.065	0.054	–
d	200	–	μm
λ	635	–	nm
Δp	3.75	–	μm
i_0	652	–	–

Table 1: Parameters mean values and standard deviations (both resulting after outliers removal) obtained in the fitting procedure of the 13,000 CCD frames. No std indicates a parameter that was fixed during the fitting procedure.

ment, this fact is translated as: if one succeeds in measuring the path of each photon by being able to tell if it crossed through the left or the right slit, then the interference component should vanish. However, when a group of untracked photons form an interference pattern, it's still possible to measure the particle-like trajectory information, but a group average instead of the individual tracks. The fit procedure previously described managed to obtain this information by extracting U_r, the ratio between the amount of light crossing each slit.

In a standard double-slit experiment, the only way to cause controlled variations in U_r is by introducing into one of the slits some physical agent to interact with the light. The proposed study extends the standard experiment by adding an extra component: a participant (also denominated as *conscious agent*) trying to mentally interact with the light and influence the slits intensity ratio. According to the present scientific consensus, the agents must play a passive role, i.e. they shouldn't be able to modify the measured interference pattern with their introspective intentional efforts. However, motivated by the empirical evidence previously described, a theoretical model is developed to identify possible experimental signatures arising in the case of a legitimate psychophysical interaction.

The interaction dynamics is modeled by a binary choice $c = \pm 1$, an intensity $0 \leq \psi \leq 1$, and a phase difference $-\pi < \phi \leq \pi$ – all functions of the conscious agent subjective state. The extended interference pattern equation accommodating the supposed psychophysical interaction is then given by:

$$I(x, c, \psi, \phi) = \left| \sqrt{\frac{1 + c\,\psi}{2}}\, U_1(x) + \sqrt{\frac{1 - c\,\psi}{2}}\, e^{i\,\phi}\, U_2(x) \right|^2 + DC, \tag{3}$$

and in more detail:

$$I(x, c, \psi, \phi) = \frac{1 + c\,\psi}{2}\, I_1(x) + \frac{1 - c\,\psi}{2}\, I_2(x) + \tag{4}$$
$$+ \sqrt{1 - \psi^2}\, \cos\left\{ \frac{k}{2y}\, \left[x_2^2(x) - x_1^2(x) \right] + \theta_r + \phi \right\} \sqrt{I_1(x)\, I_2(x)} + DC.$$

Inspecting Eq. (4) one learns that a ψ action would increase the amount of light diffracted through a specific single slit while decreasing the amount in the other. The binary c choice expresses the specific slit to be enhanced: $c = 1$ meaning slit 1 and $c = -1$ meaning slit 2. For

a non-zero ψ, the interference term decreases independently from c. A ϕ action would shift the interference term to the left/right depending on its sign.

Although it's possible to work with the time domain pattern, the information extraction using fitting procedures requires intensive computations. Facing this technical challenge, it's convenient to Fourier transform the light intensity (operation denoted as $\mathcal{F}\{I\}$) using fast algorithms and searching for the interaction signatures in the k frequency domain. The following differences in the magnitude and phase components are adopted as a metric to characterize the most sensitive wavenumbers related to ψ and ϕ variations:

$$\Delta M(k) = M_{\text{int}}(k) - M_{\text{rlx}}(k) \quad ; \quad \Delta P(k) = P_{\text{int}}(k) - P_{\text{rlx}}(k), \tag{5}$$

where $\mathcal{F}\{I(x, c, \psi, \phi)\} = M_{\text{int}} \exp(i\, P_{\text{int}})$ and $\mathcal{F}\{I(x, 0, 0, 0)\} = M_{\text{rlx}} \exp(i\, P_{\text{rlx}})$. Using the fit extracted physical parameters from Tab. (1) and Eqs. 4–5, the $\psi\phi$-interacting versus the non-interacting differences are numerically evaluated and presented in Fig. (2).

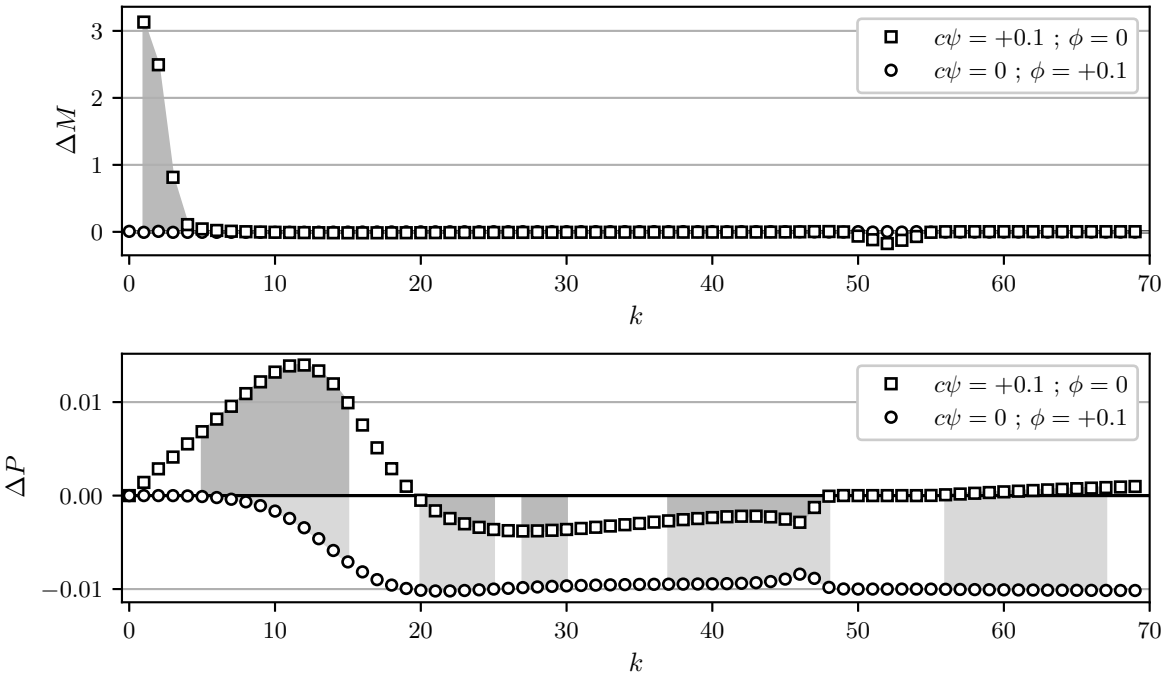

Figure 2: Magnitude and phase difference signatures for different values of c, ψ and ϕ. The magnitude shaded region represents the area explored in the real-time feedback, while the phase shaded areas represent the five chosen wavenumber regions for building the variables of interest used in the analysis. The difference curves in both plots possess an odd function symmetry regarding a c and ϕ sign inversion.

The difference signatures are used to guide the construction of variables of interest sensitive to $\psi\phi$-action. For example, a variable can be designed as the area of the magnitude component evaluated between $k = 1$ and 4. In this way, a CCD frame is translated into a single real number that should increase as ψ increases, and vice versa.

2.3 Experiments

Over a time span of 9 months starting in October 2016, 127 volunteers contributed to 160 experimental sessions following the procedure described in Section 4.3. The participant's task alternated between mentally intending the increase of light intensity crossing through a specific slit and interrupting the intention effort. Each participant session was followed by a control

session where no one was present in the experimental room. The data collection occurred across five experiments labeled from 1 to 5 with a pre-planned number of participants.

The first 20 sessions from experiment 1 were obtained in a pilot study. Using a 0.3 conservative estimative of the obtained effect size, an $\alpha = 0.05$ probability of making a Type I error, and a statistical power of 0.8, 120 sessions were calculated as a safe number for achieving this goal. This number was divided into three experiments testing different feedback configurations and later on extended to 160 to perform two additional experiments that tested a feedback test hypothesis inversion while using the same feedback variable and included more sensitive environmental measurements.

The variables of interest were built using the phase component obtained by the CCD frame Fourier transform. A higher sensibility is expected as "much of the information about the shape of the time domain waveform is contained in the (Fourier transform) phase, rather than the magnitude" [25, p. 192]. The variables k area ranges are defined through an interactive process: it starts with a model compatible k range suggestion and proceeds to analyze all the collected data with the bootstrap procedure described in Section 4.5. The initial k range is then slightly changed and the process repeated, each round resulting in a statistical score for the intention versus relax differences. The chosen k ranges are the ones revealing the higher Stouffer's z-scores for the participant data (denoted as z_p).

The optimal area ranges found for the phase variable in the current setup are: k running from 5 to 15, denoted as V_1 and followed by the notation $\langle 5-15 \rangle$ for expressing its range; V_2 $\langle 20-25 \rangle$; V_3 $\langle 27-30 \rangle$; V_4 $\langle 37-48 \rangle$; and V_5 $\langle 56-67 \rangle$. The variables are built following steps 1–5 from Section 4.5. The k removal rate per session as described in step 4 is around 6% for $V_{1,4,5}$ and 23% for $V_{2,3}$. The expected variations for the five variables in case of a $\psi\phi$-interaction are shown in Fig. (2).

		V_1 $\langle 5-15 \rangle$		V_2 $\langle 20-25 \rangle$		V_{12}				
exp.	N	z_p	z_c	z_p	z_c	comp.	z_p	z_c	es_p	es_c
0	30	0.51	-0.54	0.39	0.79	$V_1 + V_2$	0.35	0.10	0.06	0.02
1	60	-1.48	1.99	1.13	-0.32	$-V_1 + V_2$	2.13	-1.17	0.28	-0.15
2	30	0.51	0.73	1.11	-0.37	$V_1 + V_2$	1.73	0.70	0.32	0.13
3	30	1.65	-0.16	-0.94	0.27	$V_1 - V_2$	2.38	-0.43	0.43	-0.08
4	20	1.84	-0.12	-0.91	0.86	$V_1 - V_2$	2.24	-0.74	0.50	-0.17
5	20	-3.19	-0.56	-2.77	-0.97	$-V_1 - V_2$	3.48	1.39	0.78	0.31
1-5	160						**5.11**	**-0.37**	**0.40**	**-0.03**

		V_α			$V_{12\alpha}$				
exp.	N	α comp.	z_p	z_c	comp.	z_p	z_c	es_p	es_c
0	30	V_4 $\langle 37-48 \rangle$	-1.20	-0.50	$V_{12} - V_4$	0.70	0.37	0.13	0.07
1	60	V_3 $\langle 27-30 \rangle$	-1.38	-0.27	$V_{12} - V_3$	2.27	-0.89	0.29	-0.11
2	30	V_3 $\langle 27-30 \rangle$	-0.94	1.11	$V_{12} - V_3$	2.51	0.38	0.46	0.07
3	30	V_4 $\langle 37-48 \rangle$	3.17	-0.49	$V_{12} + V_4$	3.83	-0.14	0.70	-0.03
4	20	V_5 $\langle 56-67 \rangle$	2.70	1.09	$V_{12} + V_5$	2.98	-0.22	0.67	-0.05
5	20	V_4 $\langle 37-48 \rangle$	1.98	0.50	$V_{12} + V_4$	3.35	1.35	0.75	0.30
1-5	160					**6.37**	**-0.04**	**0.50**	**0.00**

Table 2: Statistical results obtained with the method described in Section 4.5. The participant (control) sessions Stouffer's z-score is denoted as z_p (z_c), while effect size is denoted as es_p (es_c). In experiment 0, the third variable selection and the compound variables sign definitions are such that it maximizes its z_p.

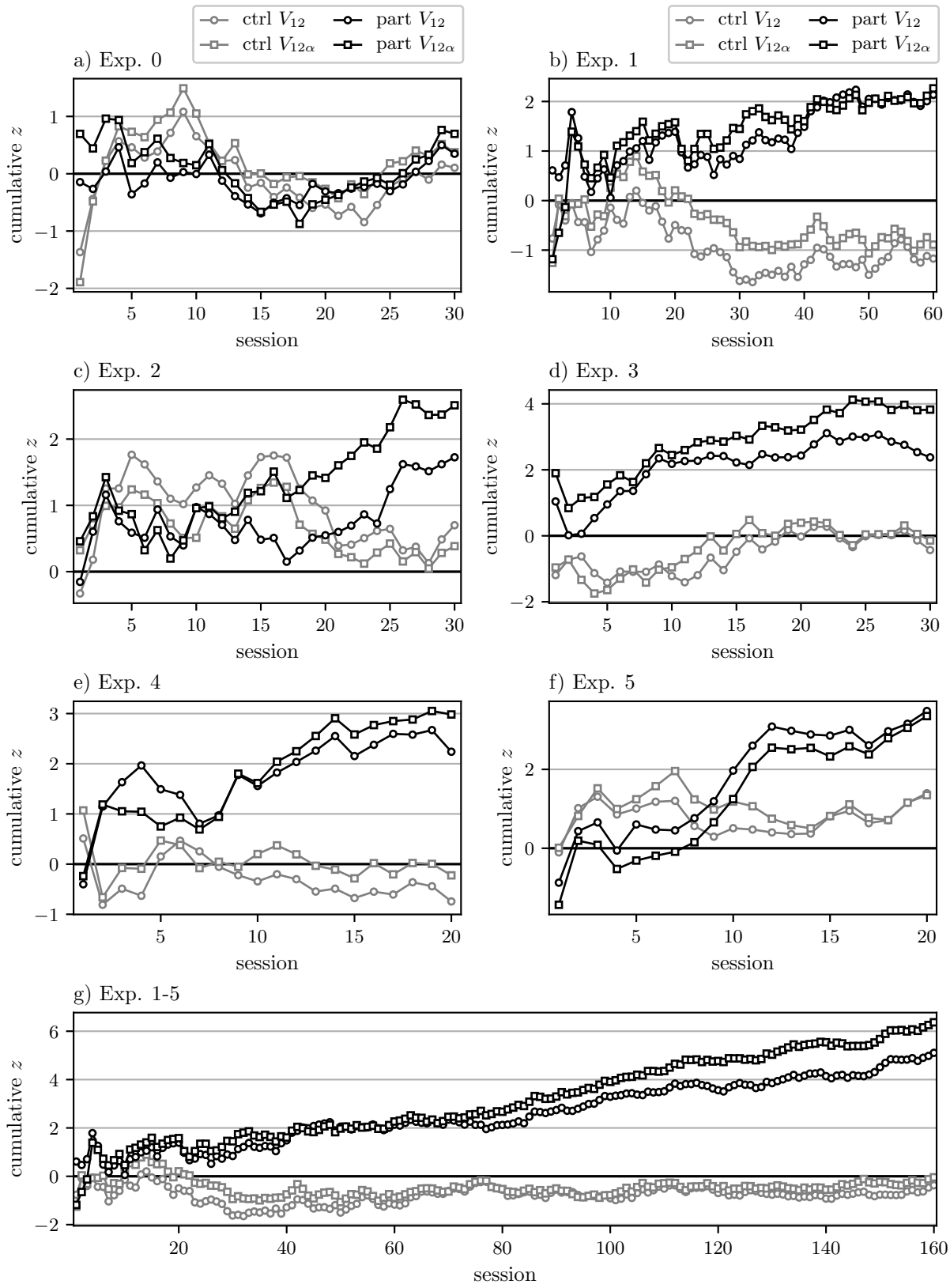

Figure 3: The cumulative z-score for each experiment calculated as $\sum_{i=1}^{s} z_i/\sqrt{s}$ and given as a function of the session number s. The last points represent the values shown in Tab. (2). Plot g) reveal the global result for the 160 sessions from experiments 1–5.

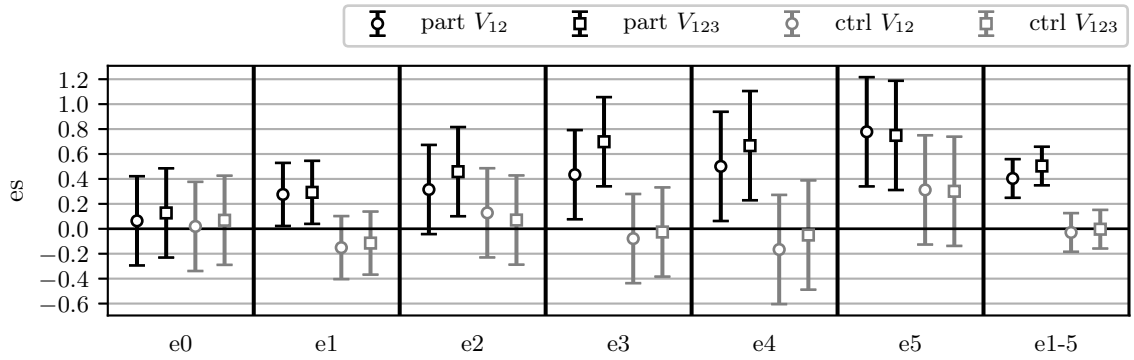

Figure 4: Effect size for all experiments. The error bars represent the 95% confidence level interval, calculated as $1.96/\sqrt{N}$, where N is the experiment sessions number.

Table 2 summarizes the statistical results obtained concerning the variables differences between the intention and relax conditions. The top table refers to the V_1 and V_2 variables used in all experiments and their composition V_{12}. The bottom table extends the compound variable to a third component, selected in each experiment for yielding the maximum z_p. The variable composition is a strategy used to enhance the signal-to-noise ratio: it increases the signal in the case of a correlated activity in the combined regions, and it washes out the noise in the case of no interaction. The different sign definitions used in the compound variables (equally applied in participant and control sessions) are understood as experiment specific relationships between the two $\psi\phi$ degrees of freedom, resulting from the distinct feedback strategies discussed in Section 2.5.

The overall results for experiments 1 to 5 consisting of z-score, associated two-tailed probability, number of positive resulting z-score sessions and effect size in the V_{12} variable are: $z_p = 5.11$, $p_p = 3.29 \times 10^{-7}$, $n_p^+ = 105$, $es_p = 0.40 \pm 0.08$ for the participant sessions and $z_c = -0.37$, $p_c = 0.71$, $n_c^+ = 79$, $es_c = -0.03 \pm 0.08$ for the controls. The overall results for the three component variable $V_{12\alpha}$ are: $z_p = 6.37$, $p_p = 1.89 \times 10^{-10}$, $n_p^+ = 112$, $es_p = 0.50 \pm 0.08$ and $z_c = -0.04$, $p_c = 0.97$, $n_c^+ = 78$, $es_c = 0.00 \pm 0.08$. The results show a significant deviation in the differential z-score obtained in the participant sessions and a null effect in the controls.

The cumulative z-scores presented in Fig. (3) reveal that the participant effects are consistently obtained in a crescent fashion across the experimental sessions, rather than being caused by a few deviating sessions. It also shows how the three variable composition (as compared to the two variable composition) enhances the z result in the participant sessions while approximating the controls to the null value. The effect sizes seen in Fig. (4) reveal a linear improvement for the V_{12} variable across the experiments and a general improvement for $V_{12\alpha}$ after experiment 2. The possible causes are discussed in Section 2.5.

In an experiment labeled as 0, 30 sessions were recorded following the exact same procedure of experiments 1-5, the only difference being a 150 W lamp replacing a person during the participant sessions. The lamp was placed in the participant chair inside a black cylindrical cardboard and was turned off before the control session started. The null effect results exclude a room temperature increase as an artifact source.

To study the $\psi\phi$-interaction homogeneity along the sessions duration, the variable residual and the condition data were sliced in half before the differential analysis. Considering experiments 1–5, the first and second half data overall results for V_{12} are $z_p^{1st} = 3.10$, $z_p^{2nd} = 3.32$ for the participant sessions and $z_c^{1st} = -0.84$, $z_c^{2nd} = 0.27$ for the controls. For $V_{12\alpha}$, it resulted in $z_p^{1st} = 5.20$, $z_p^{2nd} = 3.50$ and $z_c^{1st} = -0.65$, $z_c^{2nd} = -0.07$. The both halves significant results in the participant sessions indicate a consistent $\psi\phi$-action across the time.

In experiment 3, two CCD frames were collected in the 100 ms window. The first one

was used to provide the real-time feedback and the second one was simply stored – no effort was made to process it or to inform the participant of its variations. This design was used to investigate the supposed $\psi\phi$-interaction characteristics: if it depends exclusively on some information reaching the conscious agent or if it can be better understood as some sort of field interaction that could reach the undisplayed frame. The second frame result for V_{12} is $z_p = 2.08$, $z_c = -0.34$ and $z_p = 3.37$, $z_c = -0.44$ for V_{124}, revealing similar results to those obtained with the first frame analysis and thus favoring the second hypothesis.

The same differential analysis applied to the luminosity variable, i.e. the total amount of light reaching the CCD sensor, results in a $N = 160$ global $z_p = 1.17$ and $z_c = -0.75$, where none of the experiments showed a significant deviation. The $\psi\phi$-interaction can be seen as globally conserving the light intensity, while locally redistributing the intensities between the slits.

2.4 Environment variables

The differential analysis was applied to the environment variables (described in Section 4.2) and the resulting standard scores are presented in Tab. (3). The last three rows with A1, A2, and A3 experiments, represent three different sign composition strategies for obtaining the $N = 160$ global Stouffer's z-score: A1 corresponds to $[+1, +1, +1, +1, +1]$, where the first entry represents the value multiplied by the experiment 1 z-values, and so on for the next entries/experiments; A2 is motivated by the V_1 z-score signs, and corresponds to $[+1, -1, -1, -1, +1]$; A3 is motivated by the V_2 z-score signs, and corresponds to $[+1, +1, -1, -1, -1]$.

	T_C		T_L		T_R		$\lvert M_x\rvert$		$\lvert M_y\rvert$		$\lvert M_z\rvert$	
exp.	z_p	z_c	z_p	z_c	z_p	z_c	z_p	z_c	z_p	z_c	z_p	z_c
0	-0.08	0.41	0.22	0.12	0.88	0.24	-1.19	-0.30	0.30	0.46	**2.22**	-0.67
1	1.17	-0.33	-0.25	0.53	-0.70	-0.23	0.91	0.43	-0.34	-0.09	0.07	0.16
2	-0.69	0.91	-1.21	1.49	1.03	0.12	0.19	-0.23	0.70	-0.10	-0.83	-1.36
3	-1.14	1.28	**3.14**	-0.21	-1.61	1.35	-0.59	-1.07	**-2.12**	0.71	**2.43**	-0.18
4	-0.73	0.03	-0.68	-0.22	-0.15	0.18	-0.05	1.26	-0.10	-0.04	0.70	-0.70
5	-0.11	0.44	0.20	-1.09	-1.15	0.34	-1.24	-1.10	-1.53	0.98	-1.15	-0.63
A1	-0.37	0.91	0.52	0.41	-1.14	0.68	-0.07	-0.25	-1.40	0.54	0.58	-1.04
A2	1.73	-1.01	-0.68	-0.54	-0.53	-0.71	0.31	-0.01	-0.10	0.04	-1.30	0.79
A3	1.20	-0.53	-1.87	1.53	1.18	-0.86	1.35	0.57	1.59	-0.73	-1.21	0.06

Table 3: Differential z-score for the environmental variables across the experiments. Three different sign composition strategies (A1 to A3) were tested to obtain the global score. To investigate magnitude variations, the magnetic field components were transformed into their absolute values before analysis. Bold numbers represent the statistically significant scores.

Although experiment 3 resulted in three statistically significant values for the participant sessions, the effect was not consistently replicated across the experiments, such that no combination A1, A2, or A3 resulted in a global significant result. This excludes the trivial explanation of temperature or magnetic field variations in intention/relax conditions being the primary cause of the changes measured in the V variables.

The next step, was to check the Pearson's r correlation between the 160 differential z-scores obtained for the V variables of interest and the 160 differential z-scores obtained for the environmental variables. When looking at $V_{12\alpha}$, $|M_x|$ it's the only environment variable that shows a statistically significant correlation: $r_p = -0.24$, $p_p = 2.21 \times 10^{-3}$ for the participant sessions and $r_c = -0.05$, $p_c = 0.54$ for the controls. The V_{12} calculation showed a similar result $r_p = -0.21$, $p_p = 8.97 \times 10^{-3}$, $r_c = -0.04$, $p_c = 0.59$. For V_1, the significant correlation

appeared for T_C as $r_p = -0.17$, $p_p = 2.96 \times 10^{-2}$, $r_c = 0.00$, $p_c = 0.97$, while for V_2 appeared only for T_R as $r_p = 0.16$, $p_p = 4.91 \times 10^{-2}$, $r_c = -0.06$, $p_c = 0.45$.

The fact that the control sessions resulted in no correlations reinforces the previous argument of independence between the environment and the measured light variation. On the other hand, the significant correlations found in the participants sessions may be interpreted as some sort of physical signature resulting from the $\psi\phi$-interaction. To investigate the consistency of this claim, a second sensor system $MT2$ with a more sensitive magnetometer and a temperature sensor attached to the camera heat sink was added to experiments 4 and 5.

The same differential analysis was applied to the $MT2$ temperature $T2_C$ and magnetic field sensor variables $(M2_x, M2_y, M2_z)$, resulting in non-statistically significant single (and global) z-score for experiments 4 and 5. The 40 points correlation analysis resulted in a significant r comparing V_2 and $T2_C$ z-scores: $r_p = -0.42$, $p_p = 6.35 \times 10^{-3}$, $r_c = -0.12$, $p_c = 0.45$. Although the $MT2$ system failed to reproduce the $|M_x|$ correlation, it also displayed a negative significant correlation with the camera temperature, but in V_2 instead of V_1.

2.5 Feedback configuration

Finally, to investigate how different signs may have arisen from the different V variables across the experiments, it's necessary to understand how the real-time feedback was configured for each one. As described in Section 4.6, the feedback configuration consists of two experimenter choices: a variable of interest and a binary single-tailed test hypothesis. By fixing these choices the experimenter defines the binary c while the participant concentrates in the $\psi\phi$-action.

In experiment 5, the feedback variable was built using the log-transformed M magnitude component of the Fourier transform and defined as the area across the $k = 1$ to 4 range. The feedback hypothesis (represented by the $>$ symbol) tested an increase of the variable's mean in the short time 3 s window, as compared to the 15 s one. The larger the variable mean increase, the lower the p probability of the two-sample mean equality and hence, the larger F. The instantaneous F increase in this experiment is expected to reflect a positive $c\psi$ effect as revealed in Fig. (2), i.e. an increase in the diffraction power through slit 1. In experiment 4, the feedback is configured with the same variable but the opposite $<$ test hypothesis. In this case, an F increase is related to an enhancement in the number of photons crossing the second slit.

The definitions used in each experiment can be seen in Tab. (4). The use of different strategies for building the feedback variable over the progressing experiments translates into the learning curve of the author as the experiment evolved. Although different variables have been used, all of them explored the first two to five magnitude k wavenumbers, the most sensitive magnitude region concerning a supposed ψ action. The first experiments used a ratio, mathematically defined as $\sum_{k=49}^{55} M[n,k] / \sum_{k=1}^{4} M[n,k]$ and represented as $M\ \langle 49-55 \rangle\ /\ \langle 1-4 \rangle$ in the case of experiment 1. In practice, the nominators used in the experiments 0–3 have much smaller predicted variations as compared to the denominators. Thus, the denominators dominate the variable change in case of a ψ action, implying in an inversion between the test hypothesis and the enhanced slit: an increase in slit 2 diffraction power with the feedback $>$ hypothesis.

When analyzing the phase difference presented in Fig. (2), one finds that a $c\psi$ action is predicted to dominate the first 15 wavenumbers, while a ϕ action would be more evident from $k = 20$ onward. The V_1 z-score signal is then used to obtain from the experimental data the c value throughout the experiments. In experiments 4 and 5 for example, the same feedback variable was used but the test hypothesis inverted, resulting in inverted V_1 variable z sign in the two experiments. As shown in Tab. (4), the model predicted favored slits are maximally anti-correlated to the experimentally obtained (in experiments 1– 5). Although the negative correlation reveals a theoretical issue yet to be understood, the absolute interconnectivity of both indicate a successful single-slit enhancement control and the importance of the feedback during the data taking.

exp.	FV	FH	MS	ES
0	$M\ \langle 49-55\rangle\ /\ \langle 1-4\rangle$	$<$	1	1
1	$M\ \langle 49-55\rangle\ /\ \langle 1-4\rangle$	$<$	1	2
2	$M\ \langle 5-9\rangle\ /\ \langle 1-5\rangle$	$>$	2	1
3	$M\ \langle 3-10\rangle\ /\ \langle 1-2\rangle$	$>$	2	1
4	$\log M\ \langle 1-4\rangle$	$<$	2	1
5	$\log M\ \langle 1-4\rangle$	$>$	1	2

Table 4: Feedback configuration: variable of interest (FV) and one-tailed test hypothesis (FH); followed by the model predicted favored slit (MS) and the experimentally favored one (ES), obtained through a V_1 z-score sign inspection.

A question to be addressed concerns the effect size evolution throughout the experiments. In experiment 1, the variable nominator is associated to the peak seen in Fig. (6) M plot. It was initially imagined that the peak exclusively translated the waveness of the pattern. Afterwards, it was understood that it actually represents a convolution between the cosine waveness and the two slits diffraction term product, as a result of the Fourier convolution theorem applied to the third term of Eq. (4). The consequence for the feedback variable is a ratio between two similar information, thus blurring the variations caused by a possible $\psi\phi$-interaction. In experiment 2, an extra variable was built with the same k ranges but using the Fourier phase component. Examining the phase difference in Fig. (2), it's possible to see that the nominator dominates in this case, thus implying a slit 1 diffraction favor, while the magnitude variable favored slit 2. The z resulting from the phase and the magnitude variables were combined to calculate the feedback magnitude, leading to a contradictory slit enhancement request. In light of these arguments, it's possible to interpret the effect size increase throughout the experiments as resulting from better quality information being provided to the participant.

3 Discussion

The five experiments testing a consciousness-related form of interaction with a double-slit system resulted in a 6.37 sigma effect, successfully replicating the anomaly found by previous studies. In contrast, the control sessions conformed to the null hypothesis, showing that the obtained effect cannot be reduced to methodological or analytical artifacts. The effect neither can be explained by a temperature increase in the experimental room as shown by experiment 0 with a lamp producing more heat than a human body does. Experiment 0 also excluded possible artifacts caused by the participant/control sessions order. Care was taken in order to isolate the experiment from mechanical vibrations and electromagnetic waves, as well to monitor the magnetic field and the temperature over different places. The same differential analysis procedure resulted in no significant results for the monitored environmental variables, discarding those physical processes as the primary causal sources of the light measured intention/relax differences.

The participants intended the feedback magnitude increase, which in turn was linked to a specific feedback variable and a test hypothesis. The variable was built by taking into account a model which predicted the most sensitive wavenumber regions in the case of a legitimate interaction. With this method, the participants indirectly intended the increase in the amount of light crossing through a specific slit. The results indicate a flexible interplay between the two degrees of freedom ψ and ϕ to achieve the desired variation, revealing a goal-oriented characteristic for the $\psi\phi$-interaction. As the light luminosity is conserved, the interaction can be pictured as Maxwell's demon kind of influence, where intention plays the demon's role by "steering" some photons to the desired left/right slit.

The observed effect cannot be explained as the consequence of a measurement taking place in the participants conscious awareness. If that were the case, one should expect to see a decrease in the interference component followed by a 50/50 balanced slit intensity ratio. Differently, the results reveal a probability modulation enhancing the light passage through the desired slit. Thus the presented results don't provide a solution to the quantum measurement problem (a similar view is shared by [26] on commenting about Radin et al. conclusions). According to the experimental evidence, it is more reasonable to label the effect as an interaction adding complex numbers to the path amplitudes, which by interference leads to a change in the outcome probabilities. Instead of challenging the quantum mechanics framework and the traditional objective interpretations, the results are suggestive of a standard-model violation, pointing to the existence of a still to be elucidated fundamental force field.

A pertinent question to be addressed is: if such an effect really exists how could it have lasted consensually undetected in spite the technological breakthroughs of the last century? First, it's reasonable to expect a small cross-section; an effect too small it could go unperceived in people's daily lives, that needs proper amplification and a group of people to be statistically detected in a controlled setting. Second, by being a function of the conscious agent subjective condition, it may rely on a specific state of consciousness and an individual skill to promote it, thus not being consistently obtainable by anyone in any situation. In particular, if the effect happens to be catalyzed by states opposed to rational faculties such as thinking and the use of language, it may lead to a paradoxical situation: the more one tries to exert control in a pragmatic approach, the less they cause the phenomenon. The third reason can be argued as a consequence of the sociocultural process described by [27, Chap. 1] that led physicists to shift from philosophical interests to a more pragmatic approach motivated by post world war II military interests. While it was not uncommon to watch the quantum physics founding fathers discussing topics such as consciousness and mysticism, after the post-war technological race, the interest in such topics not only became old-fashioned but something to be avoided while following a "serious" career path. As a result, the current consensus defends that consciousness is not necessary to describe the physical world, while not introducing consciousness per se in their experiments.

Compared to the previous efforts to probe the phenomenon using random number generators, the double-slit system has the advantage of providing interference information across a spatial dimension as opposed to binary outcomes. Having more information available makes it more sensitive to the investigated $\psi\phi$-interaction. Moreover, as opposed to the usual random number generator physical processes, it allows final state interference, which allows the phase difference ϕ to play a role in the probability modulation. Regarding the double-slit variable of interest, the use of Fourier transformed variables is suggested in order to benefit from the full CCD frame instead of using the fringe visibility three pixels (the central maximum value and its adjacent minima).

Future improvements to the current double-slit setup can be achieved by focusing on strategies to improve the signal-to-noise ratio in the interference pattern measurements and to provide clearer feedback information. From the theoretical side, refinements in the interaction model can be sought in order to provide sharper variable predictions. Regarding the profound implications in the event that the observed effect is confirmed as a legitimate anomaly, replication efforts are highly advised.

4 Methods

4.1 Equipment

A semiconductor laser diode L (DL-3148-023, single mode $\lambda = 635$ nm, transverse magnetic polarization; Sanyo) is powered through a feedback driver circuit to maintain a constant 3 mW

light output power. To minimize temperature fluctuations, the laser diode is mounted on a metal structure covered with styrofoam.

As depicted in Fig. (5), the laser light passes through two slits DS etched in a metal foil (10 μm width each, centrally-separated by 200 μm; Lenox Laser). The resulting interference pattern is recorded at 10 Hz by a CCD camera C (FL3-GE-13S2M-C, 1288 x 964 pixel, 3.75 μm pixel size, 47% quantum efficiency at $\lambda = 635$ nm, 12-bit ADC; FLIR) running at room temperature with a heat sink attached to its top. An internal 1 mm width protective glass is removed from the camera to minimize refraction distortions.

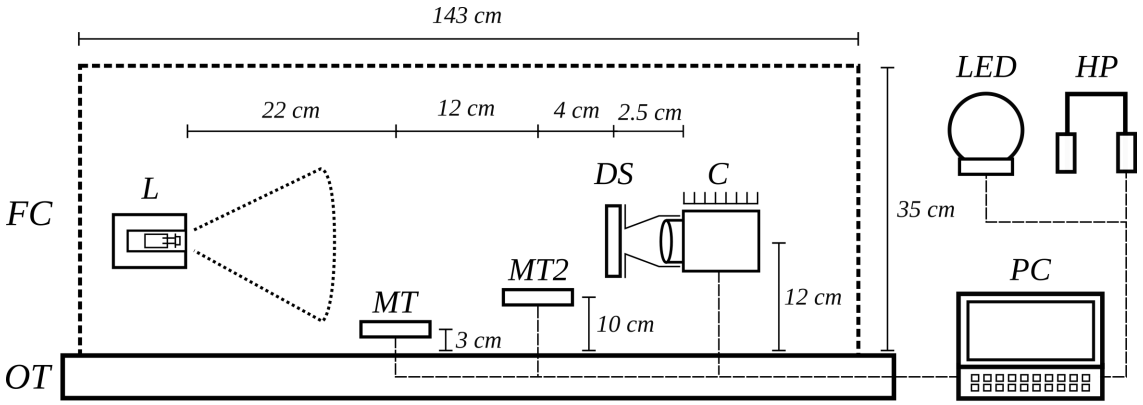

Figure 5: Experiment side view. The distance of 2.5 cm represents the separation between the double-slit and the camera wall. The distance to the camera sensor is found with a fit procedure described in Section 2.1.

A 3D-printed hollow piece is used to connect the camera to the double-slit. One extremity is firmly attached to the camera's barrel and the other to a circular metallic piece that holds the double slit foil. The plastic material color is chosen black to block light influences other than the laser.

Simultaneous to the CCD frame, temperature and magnetic field measurements are obtained using: a) an LM35 temperature sensor (0.5°C accuracy; Texas Instruments) coupled to the laser metal structure; b) an LM35 sensor placed between the laser and the double-slit for measuring room temperature ; c) an HMC5883L magnetometer (0.73 milli-gauss resolution, 12-bit ADC; Honeywell) placed close to the previous temperature sensor; d) an Arduino UNO microcontroller used to digitally read the sensors information. The whole system is presented as MT in Fig. (5).

In experiments 4 and 5, additional temperature and magnetic field measurements were obtained by the $MT2$ system consisting of: a) an LM35 temperature sensor coupled to the CCD heat dissipater; b) an HMC2003 magnetometer (0.04 milli-gauss analog resolution; Honeywell) placed close to the double-slit; c) a 4 channel 16-bit ADC (ADS1115; Texas Instruments); d) an Arduino UNO microcontroller.

The described equipments rest on a passively damped optical table OT (SmartTable UT; Newport) and inside a grounded Faraday cage FC (tombak alloy, 82% copper and 18% zinc). The experiment is controlled by a 2 GHz dual-core notebook computer PC running a custom program developed in python language. Two devices are used to provide real-time feedback for the participants: noise canceling headphones HP (QuietComfort 25; Bose) and an Arduino controlled 3W LED placed inside a spherical translucent glass. The LED is composed of three color components red, green, and blue that can be combined to produce a wide range of colors.

A grounded uninterruptible power supply (Back-UPS 2200; APC) is used to feed the computer, the CCD camera and the laser power supply (MPS-3005; Minipa, Brazil) delivering 3.3 V DC to the driver circuit. The Arduino microcontrollers are fed through the PC USB port. To ensure stable analog-to-digital (ADC) readings (concerning reference voltage variations), the following measures are taken in MT: a) the LM35 readings are obtained by the microcontroller

10-bit ADC using the regulated internal 1.1V reference; b) The HMC5883L magnetometer is connected to a power regulated circuit module. Regarding $MT2$, the LM35 and the HMC2003 are read by the ADS1115 ADC, which uses a regulated internal voltage reference.

4.2 Data acquisition

The python software controlling the experiment has its execution split into a two thread design: the first thread $T1$ is a 10 frame per second loop responsible for simultaneously triggering the sensors readings and collecting the data output within every 100 ms window; the second thread $T2$ represents the experiment flow, informing the participant about their current task, providing feedback depending on the current experimental condition, and performing data storage. As the program starts, $T1$ is set to continuously acquire data while $T2$ is in stand by mode waiting for the command to start an experimental session. As a session starts, data arrays are sequentially filled with the sensors information captured by $T1$. As the session ends, the data arrays are sent to hard-disk storage while $T1$ continues its loop and $T2$ returns to the stand by mode.

The CCD camera is configured to acquire frames using a 25 ms exposure time. Gain increase, auto-exposure and all post-processing filters (e.g. gamma, sharpness, brightness) are disabled. Each frame is initially obtained in a 1264 x per 256 z (centrally aligned) pixel window. Next, for every x, the 256 z values are summed and the result is right bit shifted by 4 units. This oversampling technique, physically viable according to the to z-axis system symmetry, is used to increase the measurement resolution from 12 to 16 bits. The resulting 1264 x values, referred to as a "CCD frame" throughout this work, represent the stored information used for the real-time feedback and the posterior analysis. Additionally, the temperature of the camera's internal components is obtained by an on-board temperature sensor (0.5°C accuracy; 12-bit ADC). Figure 6 shows an example of a single frame obtained with the current experimental setup and the interference pattern measured, as well its Fourier transform components (used for building the variables of interest described in Section 4.5).

The HMC5883L sensor is configured to 8 averaged measurements per sample and its gain is set to 0.73 milli-gauss resolution. In MT all the sensors are oversampled to reach 13-bit resolution (4 reads in HMC5883L and 64 in the LM35). In $MT2$ one single-ended ADS1115 reading (configured to a full scale-range of $\pm$ 4.096 V) is performed for each sensor resulting in an effective 15-bit resolution.

A $n = 0, 1, \ldots, n_f$ frame session results in the following data: a) a three valued condition array $C[n]$ tagging each frame to the corresponding experimental state – intention, relax, or a state in-between; b) a run array $R[n]$ filled with integers uniquely identifying the condition associated with each of the 300 frame blocks, where the blocks alternate between intention and relax conditions to a total of 40; c) a CCD frame array $U[n, i]$ with $i = 0, 1, \ldots, 1263$ and 16-bit integer values; d) the temperature arrays $T_C[n]$, $T_L[n]$ and $T_R[n]$ (32-bit floating point values) corresponding respectively to the CCD camera on-board, the laser and the room temperature sensors; e) the three direction magnetic field arrays $M_x[n]$, $M_y[n]$, $M_z[n]$ (32-bit floating point values) obtained by the MT system sensor; f) in experiments 4 and 5, the 32-bit float arrays corresponding to the CCD external temperature $T2_C[n]$ and magnetic field components $M2_x[n]$, $M2_y[n]$, $M2_z[n]$, obtained from the $MT2$ system sensors.

4.3 Procedure

To avoid potential warm-up artifacts and ensure thermal equilibrium, the following measures are taken 2 hours before every day's first session: a) laser diode and environmental sensors are turned on. In order to accelerate the CCD camera warm-up curve, it's kept power plugged in during the whole experimental block, since it maintains its internal temperature even when in stand by mode; b) the data acquisition software is started. Until the day's last session, the

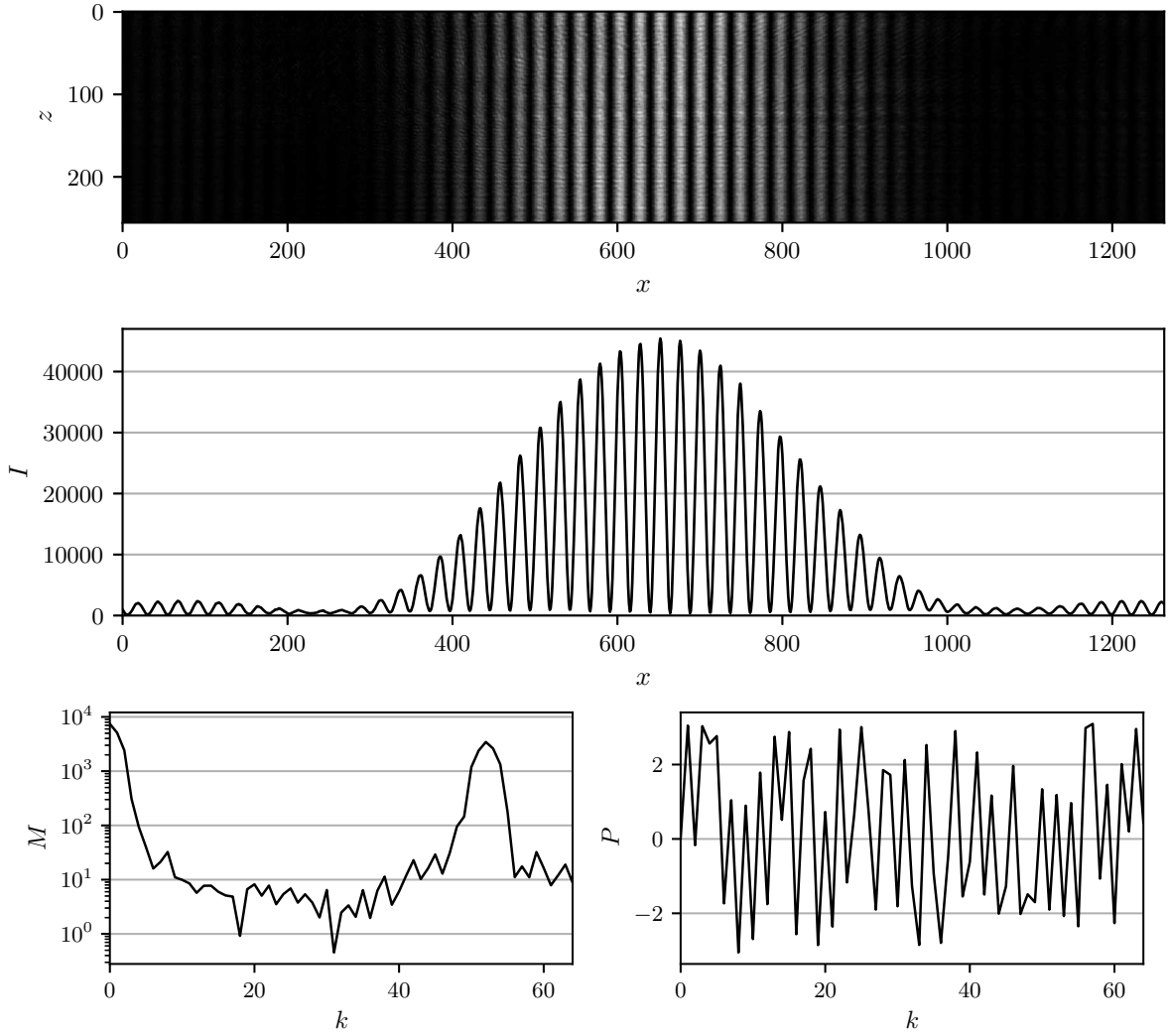

Figure 6: Single raw CCD frame showing the interference pattern measured (white color representing the pixel brightness); 16-bit oversampled one-dimensional I projection in analog digital units (the maximum value corresponds to 69% of the illumination capacity); and the log-scale M magnitude and P phase components of the respective Fast Fourier Transform.

sensors will be uninterruptedly read at 10 Hz; c) lights and air conditioning in the experimental room are switched off.

As the participant arrives at their scheduled time they fill out an informed consent form describing the nature of the experiment. Next, they read a one-page text with the task instructions to be performed. Moving to the experimental room, the participant is briefly presented with the apparatus and to the feedback devices. They sit in a chair about 3 m from the optical system, are asked to remain seated during the whole session and then to put on the noise-canceling headphones. The experimenter switches the lights off, starts the session data acquisition and leaves the room while waiting for the session end in a nearby room.

Shortly thereafter, the participant hears a headphone streamed recorded message welcoming them, followed by guided instruction to take three deep breaths. Then the recording announces the beginning of each test condition. The volunteer's task oscillates between two different situations: *intention* and *relax*. In the first, they are asked to concentrate on the intention to increase the magnitude of the provided real-time feedback (described in Section 4.6). During

the relax condition, the participant stops receiving the feedback information and is asked to temporarily cease any intention toward the experimental system. Intention runs are announced with the phrase "prepare yourself", followed by a 3-second silent delay, and then "... now, concentrate". The delay is included to allow the transition between an attention-away to an attention-toward mental state. Relax runs are announced with the phrase "now, relax". After the relax run ends, a random extra time between 0 and 5 seconds is added to the moment in-between to decouple the measurements from possible periodic oscillations.

After the session's end, the participant meets the experimenter in the next room. An automatic timer triggers a control session starting 10 minutes later, running on the exact same computer code but with no person present in the experimental room. The same decoupling time delays of the previous participant session are used.

Considering the subjective nature of the task, the participants are invited to call upon their own experiences to perform the task. However, two general guidelines are provided: they should try to avoid getting physically tired, thus acting in a present but detached way; b) they shouldn't expect to be able to exert absolute control on the feedback response. Given the random characteristics of the measurement, the feedback is supposed to show unpredictable behavior. They are informed that their influence (in really existent) could be too small to be perceived. This is important to avoid any frustration during the session and to promote a balanced state, where independent to the current feedback magnitude, the participant sustains an inflexible intent.

A single experimental session consists of 40 runs of alternating intention and relax conditions, each run lasting 30 s. Each session lasts around 28 minutes and yields approximately 16,800 sensor data frames, of which 6,000 are obtained in the intention condition and 6,000 in the relax condition. The in-between data is composed of the frames obtained during the welcome and the instructions playback, the 0-5 s random windows, and the extra 60 s collected after the last relax run. The tail data are important to absorb the polynomial fit border artifacts.

During the sessions, the experimenter had no access to the current condition nor tried to mentally influence the result. The data analysis was only performed at the end each pre-planned experimental block. Experimental sessions were scheduled on weekdays after 6 pm and on Saturdays after 2 pm, and were divided by intervals of an hour and a half, usually allowing a maximum of three (four) sessions during weekdays (Saturdays).

4.4 Participants

Participant recruiting looked for subjects interested in the investigated phenomena and that through some regular practice showed a propensity for absorptive skills. This was motivated by Radin et al. correlation results and favored meditators, mediums, holistic therapists, psychonauts, artists, martial artists, and athletes. Besides those groups, the recruiting included individuals who by their curiosity and openness were highly motivated in taking part in the experiment.

The first invitations were sent to a list of experimenter's acquaintances that met the above-mentioned group inclusion criteria. Then, some who took part in the experiment were asked to nominate new potential participants from their own acquaintances, thus implementing a snowball sampling. The biased sample offered no obstacle as the main question concerned the existence of the investigated phenomenon, regardless of effect size distortions caused by a supposedly privileged group. In particular, in an experiment which attention is a crucial ingredient, it's convenient to select volunteers who by their interest and motivation are more susceptible to perform the experimental task with an increased level of commitment.

After their selection, the recruited volunteers filled out an online form about their beliefs and experiences regarding anomalous phenomena, also including a Portuguese translated version of the Tellegen absorption scale [23]. On the session days, before and after the experimental task, they filled out a questionnaire examining their current psychological state. As previously

stated, a discussion concerning the correlations obtained between the questionnaires/scales and the experimental results are outside the scope of the present work and will be left for future publication.

Across the experiment, no tests prior to the planned sessions were performed in order to pre-select the candidates. However, 20% of the sessions consisted of returning participants re-invited by their previously obtained high z-scores.

4.5 Analysis

All the CCD frames recorded in each experimental session are processed and transformed into variables of interest according to the following steps (see Section 4.2 for the variables definitions):

1. For every n frame, the CCD frame array $U[n, i]$ is transformed by a fast Fourier algorithm and decomposed into magnitude $M[n, k]$ and phase $P[n, k]$ polar components, where $k = 0, 1, \ldots, 631$.

2. For every k, the phase is unwrapped along the n frames to $P_u[n, k]$ in a measure to remove misleading 2π discontinuities caused by the $-\pi$ to π constraint.

3. For every k, the standard deviation of $P_u[n, k]$ along the n frames is computed to $s_P[k]$.

4. A variable of interest is obtained as $V_\alpha[n] = \sum_{k=\beta}^{\gamma} P_u[n, k]$, for every k between β and γ that satisfies the $s_P[k] < 0.5$ relationship. In the case of a non-satisfying condition, the given k is left out of the sum, not contributing in that particular session to the variable. This cut is necessary to discard anomalous discontinuities that survives the unwrapping – behavior caused by the noisier P phase associated to small magnitude M values. The V_α variable is optionally followed by the notation $\langle \beta - \gamma \rangle$ to specify its area range.

5. Compound variables are built, e.g. $V_{124}[n] = V_1[n]\langle 5-15\rangle - V_2[n]\langle 20-25\rangle + V_4[n]\langle 37-48\rangle$. The specific choices concerning area ranges and sign compositions are discussed in sections 2.3 and 2.5.

A nonparametric bootstrap test is applied to the variables of interest to test the equality hypothesis between the intention and relax sample means, a procedure referred as *differential analysis*. For each session and variable, a standard z-score is obtained with the following steps:

6. An 8^{th} order polynomial is least-square fitted to the variable $V[n]$. The residual difference between the variable and the polynomial is obtained as $V_d[n]$. This nonlinear detrending procedure is made in order to rule out the variable dependency in slowly changing environmental conditions, e.g. room temperature.

7. The run array $R[n]$ is used to identify the first frame n_s of the first attention run, as well the last frame n_e of the last relax run. To avoid artifacts in the variable extremities caused by the polynomial fitting procedure, the variable V_d is trimmed in the range $n_s - 300$ to $n_e + 300$, being then denoted as $V_d[n_t]$, where $n_t = 0, 1, \ldots, n_e - n_s + 600$.

8. The condition array $C[n]$ is trimmed in the same interval (described in the previous item) to $C[n_t]$, and then is used to split the variable $V_d[n_t]$ into two arrays: $V_I[m]$ and $V_R[m]$ with $m = 0, 1, \ldots, 5999$ values respectively recorded during intention and relax conditions.

9. $V_I[m]$ and $V_R[m]$ means are calculated to μ_I and μ_R. The two-sample mean difference is denoted as $\Delta\mu = \mu_I - \mu_R$. The null hypothesis is $\mu_I = \mu_R$ while the alternative hypothesis stands for $\mu_I \neq \mu_R$.

10. A pseudorandom number r between 0 and n_t length is drawn using a Mersenne Twister algorithm. $C[n_t]$ is copied and circularly shifted by r units resulting in $C_r[n_t] = C[n_t - r]$. The procedure described in items 8 and 9 is applied to C_r, resulting in the mean difference $\Delta\mu_r$.

11. The previous item procedure is repeated 5,000 times, filling a vector with $\overline{\Delta\mu_r}$ mean and $\sigma_{\mu r}$ standard deviation.

12. The standard score concerning the intention-relax sample mean difference is obtained as $z = (\Delta\mu - \overline{\Delta\mu_r})/\sigma_{\mu r}$.

For an experiment block consisting of N sessions, a global z-score for a given variable is obtained by combining individual session results in a Stouffer's $z = \sum_{i=1}^{N} z_i/\sqrt{N}$. The effect size is then calculated by $es = z/\sqrt{N}$ with $\sigma = 1/\sqrt{N}$ standard error.

Figure 7 presents an example of a V_{124} compound variable obtained in a participant session from experiment 3. The first plot shows the variable (black line) obtained by following steps 1–5, and the associated best fitting 8^{th} order polynomial (white line). The second plot displays the variable residual (black line) as described in step 6, and (for didactical purposes) the residual average obtained through a 300 frame window SavitzkyGolay filter (white line). Both data samples are trimmed as described in step 7 and show the condition data described in step 8 – dark gray bars represent intention and light gray bars represent relax condition frames.

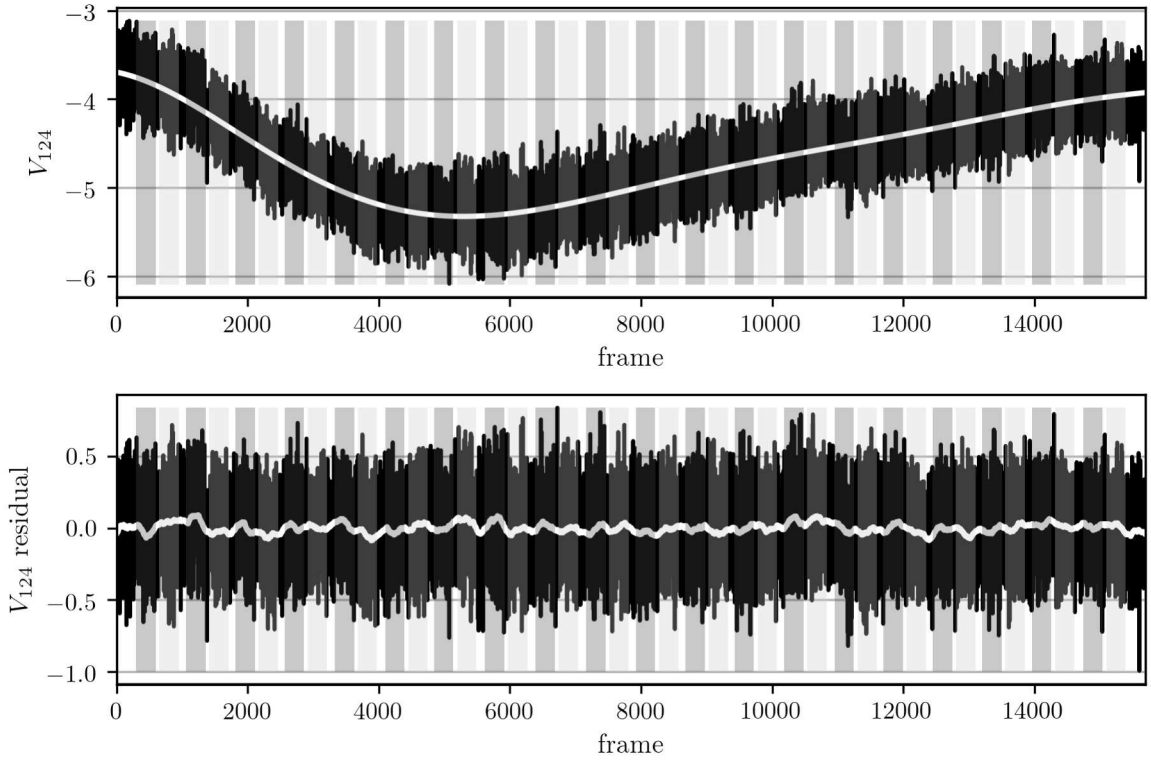

Figure 7: Variable of interest V_{124} and its residual for a participant session. This particular session resulted in a $z = 2.07$ score for this variable.

4.6 Real-time feedback

The feedback system is designed to inform the participant about variations in the two slits intensity ratio. This is accomplished by obtaining this information in real-time and then transforming it into a feedback magnitude, a real number ranging from 0 to 1 used to modulate the feedback devices intensity.

The participant is in sensory contact with two feedback devices: noise-canceling headphones playing a richly harmonic droning tone and the colorful light produced by a LED shining through translucent glass. As the feedback magnitude increases, the LED light shines more intensively in the dark experimental room, followed by the same increase in the tone volume. The feedback light colors are randomly picked for each of the 20 intention runs from a pool of 8 different pre-defined colors. During the data collection, the following method is used to calculate and inform the feedback magnitude. At every frame:

1. A fast Fourier transform is applied to the CCD frame and the magnitude component is used to calculate the (experiment specific) feedback variable of interest. For the experiment definitions see Section 2.5.

2. Two sliding window vectors are updated with the variable value, storing respectively the last 30 and 150 frame values.

3. A Mann-Whitney U test is applied to the two samples. The resulting z-score is used to calculate a one-tailed probability p. The hypothesis being tested (fixed for each experiment) is interpreted as the last 3-second variable mean being significantly greater (or less) than the last 15-second variable mean.

4. The feedback magnitude is obtained as $F = 1 - p$, and F is set to a minimal value of 0.1 if below this threshold.

5. If the current frame is associated with an intention condition, the F value is used to instantly modulate the light and volume intensity of the feedback devices. Transversely, if the experiment is in the relax condition, no information about the experiment state is given to the participant: the feedback light is kept off, and the sound is kept at a fixed $F = 0.3$ intensity. As a result, the feedback light is turned on only during intention runs, while the feedback volume is kept on during the whole session, being only modulated during intention runs and kept at a fixed 0.3 intensity during relax and during the recorded conditions announcements.

The feedback mechanism simplifies the task description, serving as an interface between the conscious agent and the physical process dynamics. Without it, the task instructions could sound rather abstract causing mental wondering and distractions during the experiment. To simplify, the participants are instructed to always intend the increase of the feedback magnitude during the intention runs. They are informed that a magnitude increase is linked to a physical variation, so by focusing on the feedback, they are indirectly interacting (or trying to) with the light crossing the apparatus. As a secondary role, the feedback is used to arouse the participants motivation as they eventually can experience some sort of correlation between the presented intensities and their subjective state, thus reinforcing their attention and intention towards the experimental system.

References

[1] D. J. Chalmers, "Facing up to the problem of consciousness," *Journal of consciousness studies*, vol. 2, no. 3, pp. 200–219, 1995.

[2] J. Von Neumann, *Mathematical foundations of quantum mechanics*. No. 2, Princeton university press, 1955.

[3] F. London and E. Bauer, "The theory of observation in quantum mechanics (1939)," in *Quantum theory and measurement* (J. A. Wheeler and W. H. Zurek, eds.), pp. 217–259, Princeton University Press, 1983.

[4] E. P. Wigner, "Remarks on the mind-body problem (1961)," in *Quantum theory and measurement* (J. A. Wheeler and W. H. Zurek, eds.), pp. 168–181, Princeton University Press, 2014.

[5] H. P. Stapp, "Mind, matter, and quantum mechanics," *Foundations of Physics*, vol. 12, no. 4, pp. 363–399, 1982.

[6] E. J. Squires, "Quantum theory and the relation between the conscious mind and the physical world," *Synthese*, vol. 97, no. 1, pp. 109–123, 1993.

[7] B. Rosenblum and F. Kuttner, "The observer in the quantum experiment," *Foundations of Physics*, vol. 32, no. 8, pp. 1273–1293, 2002.

[8] B. d'Espagnat, "Consciousness and the wigner's friend problem," *Foundations of Physics*, vol. 35, no. 12, pp. 1943–1966, 2005.

[9] H. Margenau, "Measurements in quantum mechanics," *Annals of Physics*, vol. 23, no. 3, pp. 469–485, 1963.

[10] H. D. Zeh, "On the interpretation of measurement in quantum theory," *Foundations of Physics*, vol. 1, no. 1, pp. 69–76, 1970.

[11] S. Goldstein, "Quantum theory without observers – parts one and two," *Physics Today*, vol. 51, no. 3 and 4, pp. 42–46 and 38–42, 1998.

[12] M. Schlosshauer, J. Kofler, and A. Zeilinger, "A snapshot of foundational attitudes toward quantum mechanics," *Studies in History and Philosophy of Science Part B: Studies in History and Philosophy of Modern Physics*, vol. 44, no. 3, pp. 222–230, 2013.

[13] S. Yu and D. Nikolić, "Quantum mechanics needs no consciousness," *Annalen der Physik*, vol. 523, no. 11, pp. 931–938, 2011.

[14] D. I. Radin and R. D. Nelson, "Evidence for consciousness-related anomalies in random physical systems," *Foundations of Physics*, vol. 19, no. 12, pp. 1499–1514, 1989.

[15] H. Bösch, F. Steinkamp, and E. Boller, "Examining psychokinesis: the interaction of human intention with random number generators–a meta-analysis.," *Psychological bulletin*, vol. 132, no. 4, pp. 497–523, 2006.

[16] D. Radin, R. Nelson, Y. Dobyns, and J. Houtkooper, "Reexamining psychokinesis: comment on bösch, steinkamp, and boller (2006).," *Psychological bulletin*, vol. 132, no. 4, pp. 529–532, 2006.

[17] M. Ibison and S. Jeffers, "A double-slit diffraction experiment to investigate claims of consciousness-related anomalies," *Journal of Scientific Exploration*, vol. 12, no. 4, pp. 543–50, 1998.

[18] W. K. Wootters and W. H. Zurek, "Complementarity in the double-slit experiment: Quantum nonseparability and a quantitative statement of bohr's principle," *Physical Review D*, vol. 19, no. 2, p. 473, 1979.

[19] D. Radin, L. Michel, K. Galdamez, P. Wendland, R. Rickenbach, and A. Delorme, "Consciousness and the double-slit interference pattern: Six experiments," *Physics Essays*, vol. 25, no. 2, p. 157, 2012.

[20] D. Radin, L. Michel, J. Johnston, and A. Delorme, "Psychophysical interactions with a double-slit interference pattern," *Physics essays*, vol. 26, no. 4, pp. 553–566, 2013.

[21] D. Radin, L. Michel, A. Pierce, and A. Delorme, "Psychophysical interactions with a single-photon double-slit optical system," *Quantum Biosystems*, vol. 6, no. 1, pp. 82–98, 2015.

[22] D. Radin, L. Michel, and A. Delorme, "Psychophysical modulation of fringe visibility in a distant double-slit optical system," *Physics Essays*, vol. 29, no. 1, pp. 14–22, 2016.

[23] A. Tellegen and G. Atkinson, "Openness to absorbing and self-altering experiences ("absorption"), a trait related to hypnotic susceptibility.," *Journal of abnormal psychology*, vol. 83, no. 3, p. 268, 1974.

[24] J. Goodman, *Introduction to Fourier Optics*. McGraw-Hill physical and quantum electronics series, W. H. Freeman, third ed., 2005.

[25] S. Smith, *Digital Signal Processing: A Practical Guide for Engineers and Scientists*. Demystifying technology series, Elsevier Science, 2003.

[26] M. De Bianchi, "Quantum measurements are physical processes. comment on "consciousness and the double-slit interference pattern: Six experiments" by dean radin et al.," *Physics Essays*, vol. 26, no. 1, pp. 15–20, 2013.

[27] D. Kaiser, *How the hippies saved physics: science, counterculture, and the quantum revival*. WW Norton & Company, 2011.